J Mol Model (2007) 13: 79–89
DOI 10.1007/s00894-006-0127-x

ORIGINAL PAPER

Bing Zhang · Vincent B. C. Tan · Kian Meng Lim · Tong Earn Tay · Shulin Zhuang

Study of the inhibition of cyclin-dependent kinases with roscovitine and indirubin-3′-oxime from molecular dynamics simulations

Received: 2 March 2006 / Accepted: 6 April 2006 / Published online: 13 June 2006

Abstract Molecular dynamics simulations were performed to elucidate the interactions of CDK2 and CDK5 complexes with three inhibitors: *R*-roscovitine, *S*-roscovitine, and indirubin-3′-oxime. The preference of the two complexes for *R*-roscovitine over the *S* enantiomer, as reported by the experiment, was also found by the simulations. More importantly, the simulations showed that the cause of the stronger affinity for the *R* enantiomer is the presence of an important hydrogen bond between *R*-roscovitine and the kinases not found with *S*-roscovitine. The simulations also showed two amino acid mutations in the active site of CDK5/*R*-roscovitine that favor binding-enhanced electrostatic contributions, making the inhibitor more effective for CDK5 than for CDK2. This suggests that the effectiveness of roscovitine-like inhibitors can be improved by enhancing their electrostatic interaction with the kinases. Finally, molecular mechanics–Possion–Boltzmann/surface area calculations of the CDK5/indirubin-3′-oxime system in both water-excluded and water-included environments gave significantly different electrostatic contributions to the binding. The simulations detected the displacement of a water molecule in the active site of the water-included CDK/indirubin-3′-oxime system. This resulted in a more conserved binding pattern than the water-excluded structure. Hence, in the design of new indirubin-like inhibitors, it is important to include the water molecule in the analysis.

Keywords Cycline-dependent kinase · Hydrogen bond · Binding pattern · Binding energy · Molecular dynamics simulation

V. B. C. Tan (✉) · K. M. Lim · T. E. Tay
Department of Mechanical Engineering,
National University of Singapore,
9 Engineering Drive 1,
Singapore 117576, Singapore
e-mail: mpetanbc@nus.edu.sg
Tel.: +65-68748808
Fax: +65-67791459

B. Zhang
Nanoscience and Nanotechnology Initiative,
National University of Singapore,
2 Engineering Drive 3,
Singapore 117576, Singapore

B. Zhang · S. Zhuang
Department of Chemistry, Zhejiang University,
Hangzhou 310027, People's Republic of China

Introduction

Cyclin-dependent kinases (CDKs) control the progression of the cell cycle and are a family of heterodimeric serine/threoine protein kinases comprising a catalytic CDK subunit and an activating cyclin subunit. Most CDKs have already been implicated in the regulation of the cell division cycle [1–4]. Emerging evidence further indicates that certain members of this family are also involved in other processes. For example, CDK5 has been implicated in neural development, maintenance of adult neuronal architecture, and neurodegeneration [5].

CDK5 and CDK2, cancer-treatment related CDK family members, have very similar 3-D structures, as expected from a sequence identity of 60% between them. CDK5 is composed of 292 residues and, like CDK2, is folded into a typical bilobal conformation. It has an N-terminal domain of approximately 85 residues in a mainly β-sheet structure, a predominantly α-helix C-terminal domain of about 170 amino acids, and a deep ATP-binding cleft between the two lobes. Recent investigations have revealed that CDK5 is involved in biological pathways important for several diseases, such as Alzheimer's disease, amyotrophic lateral sclerosis, Parkinson's disease etc. [6–10]. This has generated a marked interest in the search for CDK5 inhibitors [7, 11, 12]. Several reviews dealing with small molecule inhibitors have been published [12–15]. Some of these inhibitors were reported to inhibit several CDKs with different inhibitory efficiencies. (*R*)-roscovitine [2-(*R*)-(1-ethyl-2-hydroxy-ethylamino)-6-benzylamino-9-isopropyl-purine] (Fig. 1a) containing an asymmetric carbon is a purine analogue that has been shown to inhibit CDKs

potently with inhibitory concentration (IC_{50}) values ranging from 0.16 μM (for CDK5), 0.70 μM (for CDK2) to over 100 μM (for CDK4 and CDK6) while maintaining good selectivity with respect to a number of other kinases [16]. The *R*-enantiomer, however, shows higher inhibitory activity than the *S*-type for CDK1 and CDK2 [3]. Indirubin-3′-oxime (Fig. 1b) is also a potent inhibitor of both CDK5 (IC_{50} of 0.10 μM) and CDK2 (IC_{50} of 0.44 μM). It is derived from indirubin, which is the key constituent of the traditional Chinese leukemia drug Danggui Longhui Wan [15, 17]. The rigid and multi-interacting sites on the 3-D structure of the indirbuin analogues are normally ideal, structural-based drug design templates that have attracted a lot of interest in the search for new indirubin-like compounds as potent antitumor drugs [15].

The crystal structures of CDK2-roscovitine and CDK2-indirubin analogues indicate that both inhibitors are strongly bound in the ATP-binding pocket of CDK2 with similar binding patterns. However, this binding pattern is different from that of the CDK2–ATP complex [17, 18]. Due to the lack of information on the crystal structures of CDK5–inhibitor complexes, the binding modes of both (*R*)-roscovitine and indirubin-3′-oxime with CDK5 remained undetermined for a long time until recently, when Mapelli et al. reported the crystal form of CDK5/p25 with (*R*)-roscovitine, aloisine and indirubin-3′-oxime [18]. Molecular dynamics (MD) simulations were performed to find out why structurally analogous inhibitors displayed significantly different levels of inhibition with the two kinases despite the strong resemblance in the structures of CDK5 and CDK2, and the similarities in the way they bind to inhibitors. It has been highlighted that dynamic studies on binding modes are necessary for understanding key structural features and interactions, knowledge of which is essential in the design of new efficient inhibitors [19]. In the past decade, only a few theoretical studies on CDKs based on molecular dynamics simulations and quantum mechanical calculations were carried out to supplement the tremendous amount of experimental work because crystal structures of the CDK inhibitor were unavailable [19–26]. Consequently, some molecular dynamics simulations are based on homology models [21]. Here, we give the results of five molecular dynamics simulations on CDK5 and CDK2 complexes with *R*-roscovitine, *S*-roscovitine, and indirubin-3′-oxime. Throughout the manuscript, the molecules of the complexes are identified according to the labeling used in Fig. 1.

By comparing the hydrogen-bonding patterns of various pairs of kinase and inhibitor from our simulation and taking into consideration previously reported experimental results, we hope to predict whether CDK5, like CDK2, also has a stronger affinity for the *R*-roscovitine than its *S*-enantiomer. We also elucidate the inhibition efficiency of the three inhibitors on CDK5 and CDK2 to gain further insights into the structural basis for chemical inhibition by analyzing the hydrogen bonds, van der Waals and electrostatic contributions in CDK2/*R*-roscovitine, CDK5/*R*-roscovitine, and CDK5/indirubin-3′-oxime. Such analyses will aid the discovery of new and better inhibitors.

Materials and methods

Molecular dynamics simulations

Molecular dynamics simulations were carried out using the SANDER module of AMBER 8.0 with the all-atom force field by Cornell et al. [27]. Before the MD simulations, the values for some of the force field parameters for the ligands had to be developed because of the lack of reported data. Optimization of the five ligands were first achieved with the Gaussian98 package at the HF/6-31G* theoretical level. Electrostatic potentials (ESP) were then generated with Merz–Singh–Kollman van der Waals parameters [28]. Fitting of the charges to the ESP was performed with the restrained ESP (RESP) program [29] of the AMBER package. GAFF [30] force fields parameters and RESP partial charges were assigned using the ANTECHAMBER module.

The starting geometries for the simulations of the CDK5/*R*-roscovitine and CDK5/indirubin-3′-oxime were generated from the X-ray structures obtained from the Protein Data Bank (PDB ID codes are 1UNL and 1UNH, respectively.) The crystal structure of CDK2/*R*-roscovitine was provided by Prof. Laurent Meijer (CNRS, Station Biologique, France) and Dr. Sung-Hou Kim (University of Berkeley, USA). The complex structures of CDK5/*S*-

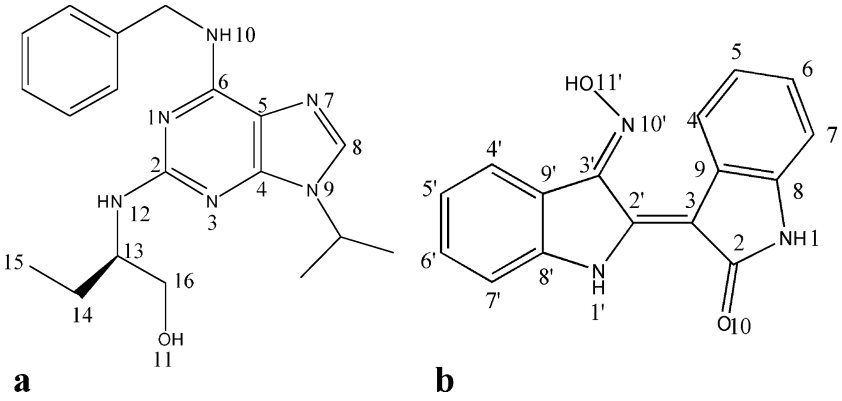

Fig. 1 Schematic representation of the *R*-roscovitine (**a**) and the indirubin-3′-oxime (**b**)

roscovitine and CDK2/*S*-roscovitine were then built using 1UNL and CDK2/*R*-roscovitine, respectively, as templates. All the modifications were made with the DS modeling program (Accelrys, San Diego, 2003). This approach of using structurally similar compounds was adopted to facilitate the construction of each protein–ligand complex and help ensure that the ligands are placed in a reasonable starting conformation. Seventeen chloride counterions were added to maintain the electroneutrality of all the systems. Each system was immersed in a 10-Å layer truncated octahedron periodic water box. The layer of water molecule in all cases contained around 1,1000 TIP3P [31] water molecules in each of the complexes. A 2-fs time step was used in all the simulations, and long-range electrostatic interactions were treated with the particle-mesh Ewald (PME) procedure [32] using a cubic B-spline interpolation and a 10^{-5} tolerance for the direct-space and with a 12-Å non-bonded cutoff. Bond lengths involving hydrogen atoms were constrained using the SHAKE algorithm [33]. All systems were minimized before the production run. The minimization, performed with the SANDER module under constant volume condition, consists of seven steps. All heavy atoms in both proteins and ligands were restrained with decreasing forces of 500, 200, 100, 50, 5, and 1 kcal mol^{-1}. In the first three steps, minimization of the solvent molecules and hydrogen atoms of the systems involved 250 cycles of steepest descent followed by 250 cycles of conjugate-gradient minimization. In the next three steps, 100 cycles of steepest descent minimization were performed followed by 500 cycles of conjugate-gradient minimization. All systems were then relaxed by 500 cycles of steepest descent and 1,000 cycles of conjugate-gradient minimization. After the relaxation, the systems were heated to 300 K. The production part of all the systems took 1 ns. The results were analyzed using the PTRAJ module in AMBER.

Molecular mechanics–Possion–Boltzmann/surface area calculations

Binding free energies of all the systems, except the two *S*-roscovitine ones, were analyzed using the molecular mechanics–Possion–Boltzmann/surface area (MM-PBSA) [34] approach to highlight the electrostatic and van der Waals contributions in the binding of the inhibitors and the proteins.

The binding free energies(ΔG_{bind}) were computed as:

$$\Delta G_{bind} = \Delta G(complex) - [\Delta G(protein) + \Delta G(ligand)] \quad (1)$$

$$\Delta G_{bind} = \Delta E_{gas} + \Delta \Delta G_{solv} - T\Delta S \quad (2)$$

$$\Delta E_{gas} = \Delta E_{int} + \Delta E_{ele} + \Delta E_{vdw} \quad (3)$$

$$\Delta G_{solv} = \Delta G_{pb} + \Delta G_{nonpolar} \quad (4)$$

The sum of molecular mechanics energies, ΔE_{gas}, can be divided into contributions from internal energy (ΔE_{int}), electrostatic potential (ΔE_{ele}), and van der Waals (ΔE_{vdw}) potential. The solvation free energy (ΔG_{solv}) is composed of two parts—polar solvation free energy (ΔG_{PB}) and nonpolar solvation free energy ($\Delta G_{\text{nonpolar}}$). All energies are averaged along the MD trajectories.

Three snapshots of the solute in each system were sampled from different parts of a single trajectory with different intervals. E_{gas} was obtained using SANDER and estimation of ΔG_{PB} was conducted with a built-in module, PBSA in AMBER. G_{nonpolar} was determined from Eq. 4 using the MOLSURF program [35, 36].

$$\Delta G_{nonpolar} = 0.00542SASA + 0.92 \quad (5)$$

Results and discussion

Determination of the initial relaxation time

The root-mean square deviation (RMSD) of the positions for all backbone C_α atoms from their initial configuration as a function of simulation time for all the systems is shown in Fig. 2. The RMSD is calculated to check whether convergence of the MD was obtained and if the MD trajectory is stable. The equilibration times section for all the systems are reported in Table 1. The values in Table 1 show that all the RMSDs fluctuate around a certain level after the stationary point is attained in each trajectory. Stella and Melchionna [37] pointed out that the common practice of using RMSD with respect to the initial structure to

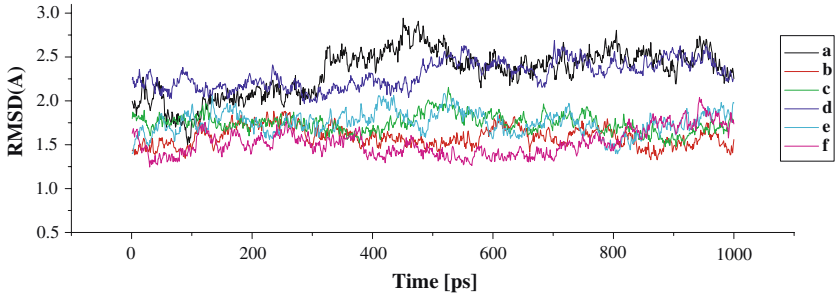

Fig. 2 Time-dependent Cα RMSD of all the complexes with respect to the initial structures for CDK5/*R*-roscovitine (**a**), CDK5/indirubin-3′-oxime (**b**), CDK2/*R*-roscovitine (**c**), CDK2/indirubin-3′-oxime (**d**), CDK2/*S*-roscovitine (**e**), and CDK5/*S*-roscovitine (**f**)

determine the initial relaxation time often overestimates the relaxation time, which results in valid simulation data being discarded. By tracing the RMSD curves backward in time, one can better identify the attainment of the stationary state in a simulation. We applied this approach for our analyses and compared the results with those derived from the customary approach. Taking the results in Fig. 3 for the CDK5/indirubin-3′-oxime complex as an example, we confirm from Fig. 3a that a stationary state is attained after approximately 170 ps, which is much shorter than if the relaxation time is calculated from the initial structure (about 300 ps, Fig. 3b). We, therefore, collected data from 170 ps onwards (Table 1).

Binding mode of the inhibitors

Two crucial hydrogen bonds (HBs), N^{10}–H777O (Leu83 in CDK2, Cys83 in CDK5) and N^{7}777H–N (Leu83 in CDK2, Cys83 in CDK5), which were reported to play key roles in the binding of roscovitine with CDK2, [3] as well as a third single HB, O^{11}–H777O (Gln131 in CDK2, Gln130 in CDK5), were all found in our simulations for both CDK5 and CDK2 complexes (Fig. 4), demonstrating that the molecular dynamics simulation results are in agreement with experimental data. The rotations of two torsions (N^{12}–C^{13}–C^{14}–C^{15} and N^{12}–C^{13}–C^{16}–O^{11}) at the C^{2} side chain observed in Otyepka et al.'s simulations [20] were also detected in our CDK2/*R*-roscovitine simulation. However, in the CDK5/*R*-roscovitine simulation, the torsions remained stable throughout the whole process. As a result of the torsional rotations, the two *R*-roscovitines share a similar conformation and occupy almost the same location in their respective receptors. HBs between the inhibitor and the residues at the active site are reported in Table 2. From Fig. 4 and Table 2, it is obvious that the two complexes share the same pattern of HB networks in both proteins at the same three binding sites. Moreover, the corresponding HBs for the two kinases have very close HB lengths. We started our simulations on *S*-roscovitine systems from the same initial coordinates as their enantiomer's complexes with the only modification being the change in the *R*-conformation inhibitor to the *S*-conformation. HBs in these systems are also reported in Table 2. Analysis of these HBs indicates that there is no formation of a third HB O11H777O(Gln130) due to the repositioning of the hydroxyl in both *S* systems unlike in the *R* systems (Fig. 5). However, the two *S* systems still share the same HB pattern, just as in their enantiomer complexes. Despite the absence of a third HB, we still monitored the distance between the O^{11}–H and the oxygen of Gln130 in the time-averaged structures of both complexes and found that the distances are up to 4.46 Å for CDK2/*S*-roscovitine and 5.72 Å for CDK5/*S*-roscovitine. These distances are too long for HBs to form.

In terms of bond orientations and bond lengths, there is no obvious difference between the hydrogen bonds in CDK5/*R*-roscovitine and their counterparts in CDK2/*R*-roscovitine. Hence, HB is unlikely to be the reason why *R*-roscovitine is more effective for CDK5 (IC_{50}=0.16 μM) than CDK2 (IC_{50}=0.45 μM). Similarly, one cannot predict on which protein the *S*-enantiomer will be more effective by examining HB distributions on their own. It is clear from Figs. 4 and 5 that only the hydrogen of the chiral hydroxyethyl substituent of *R*-roscovitine can be hydrogen-bonded to the main chain carbonyl oxygen of Gln130, whereas the hydroxyethyl group in *S*-isomer is too far away (4.46 Å) to reach the oxygen. The other two HBs in CDK2/*S*-roscovitine are well-conserved between CDK2 and CDK5 complexes. HBs are much stronger than van der Waals or electrostatic interactions in ligand and protein bindings. The IC_{50} value for *S*-roscovitine (0.90 μM) is higher than for its stereoisomer when inhibiting CDK2 because of the loss of just one important HB. We can also expect CKD5 to prefer the *R*-stereoisomer over the *S*-stereoisomer. The same preference for the *R*-roscovitine has also been detected in CDK1 [3].

Unlike roscovitine, a purine analogue, indirubin-3′-oxime belongs to an oxoindole family [12, 15]. Several papers that deduced information from X-ray crystal structures of indirubins have been published [17, 38, 39]. Details of the HBs are also shown in Table 2. There are three regular HBs that the indirubin skeleton makes directly with the backbone of the kinase, just as in CDK2-indirubin-3′-oxime: the lactam amide nitrogen N^{1}H of the inhibitor donates a HB to the peptide oxygen of Glu81, the NH group of Leu83 of CDK5 donates a HB to the lactam amide oxygen O^{10}, and the cyclin nitrogen $N^{1'}$H acts as a HB bond donor to the backbone oxygen of Leu83. The main difference from the roscovitine systems is that indirubin-3′-oxime forms two additional HBs because the hydroxyl group $O^{11'}$H of indirubin is indirectly hydrogen-bonded to the side chain of Gln130 via a bridging water molecule. These water-bridged HBs are, however, somewhat different from those in the crystal structure reported by Mapelli et al., [18] in which the hydroxyl group is bonded to the side chain of Asp86 through the water. This will be discussed later.

Table 1 Equilibration times obtained from both trace-back and customary analyses

	Trace-back analysis (ps)	Customary analysis (ps)
CDK5/*R*-roscovitine	400–1,000	600–1,000
CDK2/*R*-roscovitine	500–1,000	700–1,000
CDK5/*S*-roscovitine	400–1,000	500–1,000
CDK2/*S*-roscovitine	350–1,000	500–1,000
CDK5/indirubin-3′-oxime	170–1,000	300–1,000

Mutations of amino acids in the active sites and van der Waals and electrostatic contributions

Many experiments have been performed to compare the interactions among different types of inhibitors and CDKs [40–42], and it has been found that the interaction pattern is

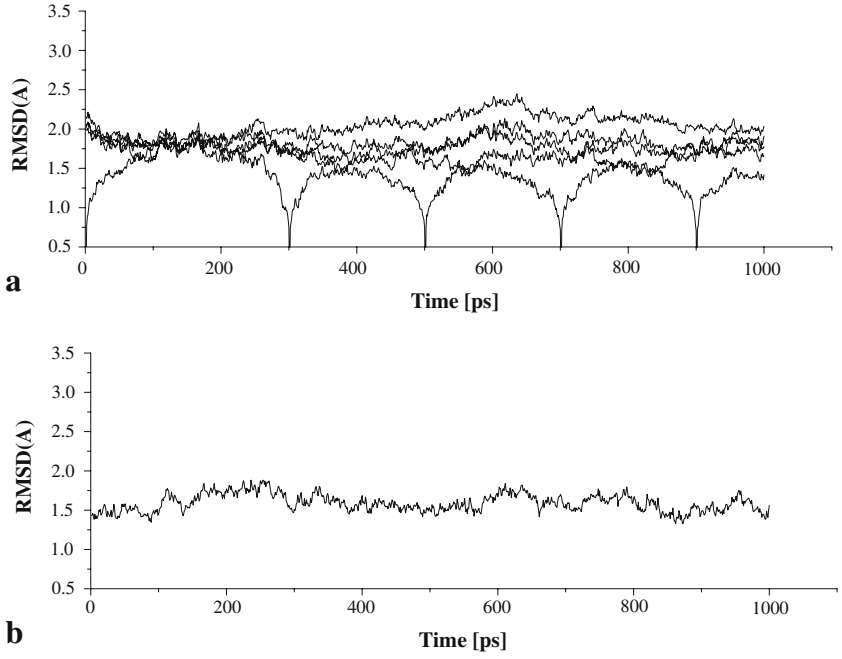

Fig. 3 RMSD of CDK5/indirubin 3′-oxime from trace-back analysis (**a**) and with respect to initial structure (**b**)

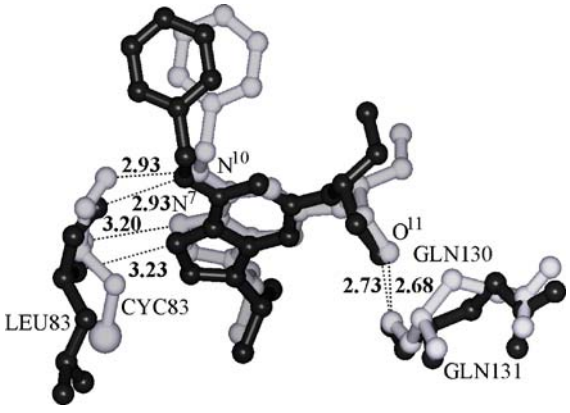

Fig. 4 Hydrogen bonding networks at the active sites of both CDK5/*R*-roscotivine (*light gray*) and CDK2/*R*-roscovitine (*black*). The labels (N^{10}, N^{7}, O^{11}) are indicated in Fig. 1

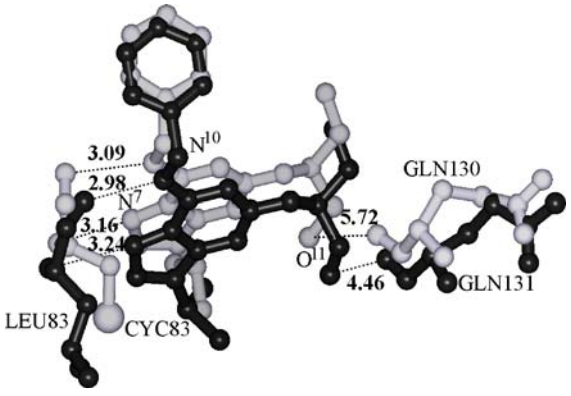

Fig. 5 Hydrogen bonding networks in the active site of both *S*-roscovitine complexes. CDK5/*S*-roscovitine is colored *light gray*, while CDK2/*S*-roscovitine is *black*

Table 2 Hydrogen bonds between the inhibitors and the active sites as obtained from simulations

Complex	Hydrogen bond	Duration[a]	Mean distance (Å)	Mean angle (°)
CDK5/*R*-roscovitine	N^{10}H777O(Cys83)	94.57	2.933	39.98
	N^{7}777HN(Cys83)	88.82	3.201	27.68
	O^{11}H777O(Gln130)	84.38	2.725	21.45
CDK2/*R*-roscovitine	N^{10}H777O(Leu83)	99.20	2.925	35.06
	N^{7}777HN(Leu83)	80.93	3.244	22.11
	O^{11}H777O(Gln130)	95.53	2.676	17.24
CDK5/*S*-roscovitine	N^{10}H777O(Leu83)	77.11	3.097	45.07
	N^{7}777HN(Leu83)	90.46	3.162	21.66
CDK2/*S*-roscovitine	N^{10}H777O(Leu83)	98.44	2.978	36.19
	N^{7}777HN(Leu83)	82.88	3.236	25.24
CDK5/indirubin-3′-oxime	N^{1}′H777O(Leu83)	40.79	3.046	45.40
	O^{10}777HN(Leu83)	99.64	2.795	20.81
	N^{1}H777O(Glu81)	96.39	3.070	19.58
	O^{11}′H777O(WAT)	71.60	2.706	16.00
	OH(WAT)777O(Gln130)	60.65	2.757	20.94

[a]Percentage of equilibration simulation time

well-conserved despite the variety of the CDKs. Almost all of the CDK inhibitors are now known to have the same mode of action—competing with ATP for the kinase binding site [38, 43]. There are around 20 key amino acids that take part in van der Waals and electrostatic interactions in the active site within CDK2/inhibitor complexes. These important amino acids in CDK2 are Glu8, Lys9, Ile10, Glu12, Gly13, Val18, Ala31, Lys33, Phe80, Glu81, Phe82, Leu83, His84, Lys89, Gln131, Asn132, Leu134, Ala144, Asp145, and Phe146. Our analyses show that among these 20 residues, three underwent mutations—Leu83, His84, and Asp145 in CDK2 mutated to Cys83, Asp84, and Asn 144 in CDK5, respectively. These may be responsible for the inhibition differences between roscovitine on CDK5 and CDK2. Asp145 is mutated to asparagine to avoid apparent toxicity from unregulated CDK5 activity in the experiments, so it is not a natural mutation. However, we still take this mutation into account in our analyses. Van der Waals and electrostatic binding energies in the two *R*-roscovitines and the indirubin-derivative systems using MM-PBSA were calculated to study variations in the binding modes caused by the amino acid mutations at the active sites. Because MM-PBSA calculations are sensitive to the stability of the simulation trajectory, three snapshots of the solute in each system were sampled from different parts of a single trajectory at different intervals. We compared the relative contributions of the van der Waals and electrostatic contributions to the total binding energy to highlight which is dominant. The percentage of binding energy due to electrostatic interactions, $\mathrm{ELE\%} = E_{\mathrm{ele}}/(E_{\mathrm{ele}} + E_{\mathrm{vdw}})$, is used as an indicator to elucidate the difference in the binding patterns between these two pairs of complexes. The van der Waals and electrostatic contributions in each system are shown in Table 3.

As mentioned above, the three mutations in the active sites are (1) Cys83 in CDK5, a weakly polar amino acid that can act as a good HB donor or a moderate HB acceptor in place of the apolar Leu83 in CDK2, which interacts with the inhibitor through van der Waals interactions; (2) Asp84 in CDK5, a negatively charged basic amino acid, substituted His84 in CDK2, which is positively charged; and (3) Asp145 in CDK2 mutated to Asn144 in CDK5. The Leu to Cys mutation implies that the van der Waals contribution at this site in CDK5 is lowered, while electrostatic interactions are improved. The mutation has no influence on HBs according to Table 2, where $N^{10}H$ and N^{7} of roscovitine can alternatively form a hydrogen bond to the backbone O and HN of the Cys83, with HB angle and length very similar with those in CDK2/*R*-roscovitine. Although the amino acids involved in the other two mutations did not participate in the formation of HBs, our observations on these residues confirm that they do influence the binding via impacting the electrostatic environment at the active site. As for the Asp to His mutation, we investigated the orientations of the positively charged His84 and the negatively charged Asp84 relative to the roscovitine in both complexes. As indicated in Fig. 6, the two amino acids are located at the same sites relative to the inhibitor, and the carbonyl group approaches the benzyl group of the roscovitine. The electrostatic potential surface model of *R*-roscovitine (not shown here) indicates that the benzyl region is a positively charged area. Therefore, it has a stronger affinity for negatively or neutrally charged groups than positively charged ones. Thus, with the substitution, the initial repulsive interaction in CDK2 was altered to an attractive one in CDK5, which undoubtedly favors the binding. Our examination of the Asp145 to Asn144 mutation yielded findings similar to those arising from the His/Asp mutation. Figure 6 shows that the side chains of both amino acids stretch toward the purine ring area of the inhibitor, a negatively charged region, as indicated in the electrostatic potential surface model of *R*-roscovitine. Thus, it is energetically more favorable to have a neutral amino acid around it than a negatively charged one.

Previous studies on CDK2/*R*-roscovitine reported that van der Waals contributions to the binding energy are more dominant than electrostatic interactions [3]. This is also validated by our MM-PBSA calculations. As seen in Table 3, the ELE% is always lower than 50% for this system. However, the above discussion suggests that the three electrostatically favorable mutations in CDK5 enhance the effect of electrostatic contributions compared to those in the CDK2 system. Table 3 shows that, in all cases for the CDK5/*R*-

Table 3 Electrostatic (E_{ele}) and van der Waals (E_{vdw}) contributions (in kilocalories per mole) for all the systems

	Time section (ps)	Internal (ps)	MM/PBSA		
			E_{ele} (kcal mol^{-1})	E_{vdw} (kcal mol^{-1})	ELE% (%)
CDK5/*R*-oscovitine	400–600	2	−27.88	−46.11	37.68
	600–800	5	−27.96	−46.08	37.76
	800–1,000	2	−28.01	−45.00	38.63
CDK2/*R*-oscovitine	500–600	2	−24.56	−44.93	35.34
	600–800	5	−25.54	−47.12	35.15
	800–1,000	2	−26.35	−46.08	36.38
CDK5/indirubin-3′-oxime (with the water)	400–600	2	−32.19	−35.59	47.49
	600–1,000	5	−31.66	−35.98	46.80
	600–1,000	2	−30.47	−36.45	45.53
CDK5/indirubin-3′-oxime (without the water)	200–400	2	−21.74	−38.56	36.05
	600–1,000	5	−20.56	−38.64	34.73
	600–1,000	2	−21.11	−38.56	35.38

$\mathrm{ELE\%} = E_{\mathrm{ele}}/(E_{\mathrm{ele}} + E_{\mathrm{vdw}})$

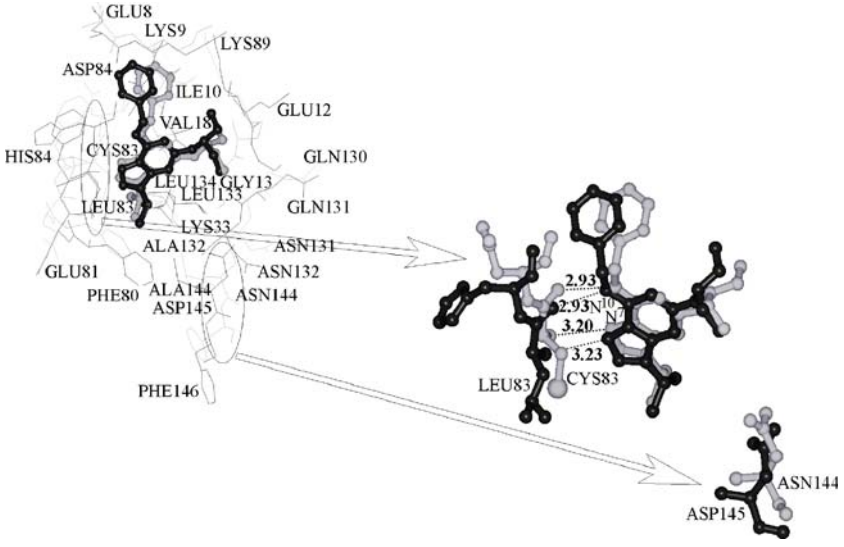

Fig. 6 Amino acids around the active sites of CDK5 and CDK2 (*top left*; amino acids are described with *lines* and roscovitine with *ball and stick*). The three pairs of mutations are separated in the *bottom right figure*, in which, roscovitine and the three mutated amino acids in CDK2 and CDK5 are colored *black* and *light gray*, respectively

roscovitine, the van der Waals interaction is still dominant, but it is noted that the ELE% of CDK5/*R*-roscovitine (38.63, 37.76, and 37.68%) is higher than that of CDK2/*R*-roscovitine (36.38, 35.34, and 35.15%). This implies that the electrostatic contribution is clearly improved because of the three mutations, although it is not dominant and not large enough to influence significantly the selectivity on CDKs. Nevertheless, this suggests that one way to improve *R*-roscovitine-like inhibitors is to modify the purine analogue to obtain structures that are more electrostatically complementary to the active site of the CDK5.

Water-bridged HB network in CDK5/indirubin-3′-oxime

In CDK5/indirubin-3′-oxime, the inhibitor also binds to the region of the pocket occupied by the ATP adenine ring and forms three HBs with the CDK5 backbone at the hinge region similar to the binding mode in CDK2 [3]. The N^1 and O^{10} atoms of the indirubin analogue form HBs with the backbone oxygen of Glu81 and the NH group of Leu83, resembling interactions observed in the complexes between monomeric CDK2 and the ATP ligands, and the staurosporine [42] inhibitor and the other two indirubin analogues [39, 44]. A third HB is formed between the indirubin-3′-oxime $N^{1'}$ and the backbone oxygen of Leu83. However, the duration of this interaction, as shown in Table 3, is only 41% of the production run, so it may not contribute very significantly to the binding affinity. This hydrogen bond has been shown to be relatively unimportant in binding studies of a CDK2–cyclinA/indirubin-5-sulfonate crystal structure [38] and in O6-substitued purines and pyrimidines complexes [45]. The difference between our simulations and previously reported experiments is that the water-bridged HB network (which exists between the hydroxyl group of the inhibitor and the side chain of Asp86 via a bridging water molecule according to the crystal structure) is replaced by a hydroxyl–water–Gln130 network. The binding in CDK2 and CDK5-

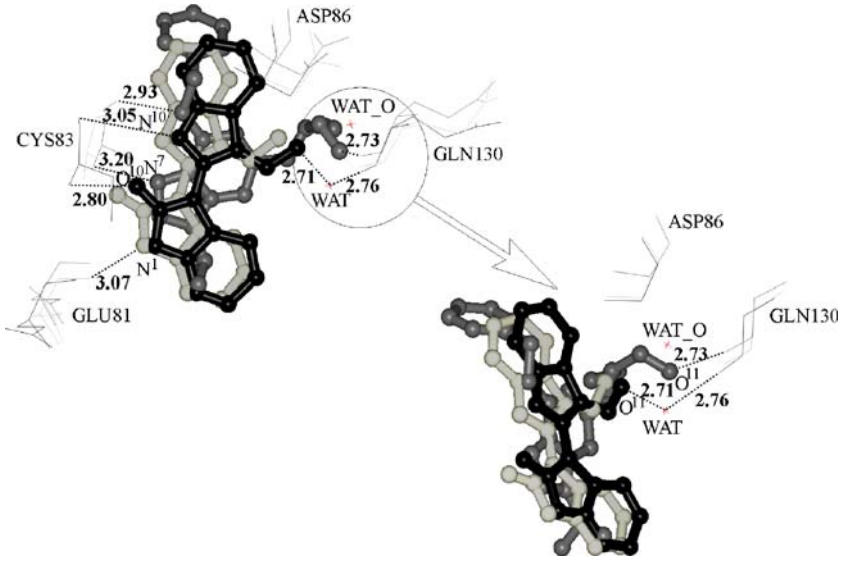

Fig. 7 Superposition of the crystal (*light gray*) and the average (*black*) structures of CDK5/indirubin-3′-oxime on the CDK5/*R*-roscovitine average structure (*dark gray*). *WAT_O* refers to the original water position and *WAT* refers to the water molecule after its displacement. The distance between the two oxygen atoms of the water is 2.52 Å. For clarity, the amino acids presented in *lines* and *sidechains* of amino acids in the *bottom right figure* are omitted

inhibitor complexes often involves Cys83 (or Leu83) and Gln130 (Gln131, in CDK2) to form three hydrogen bonds. The binding mode in this indirubin-derivative system is more similar to that in CDK5 and CDK2/*R*-roscovitine after the water molecule moves 2.52 Å toward the center between the Gln130 and the inhibitor (Fig. 7). In Fig. 7, the crystal and the average structures of CDK5/indirubin-3′-oxime and the CDK5/*R*-roscovitine average structure are superimposed. Only the inhibitors and the relevant residues are shown for clarity. It is discovered that the water molecule indeed occupied such a location that is occupied by the oxygen (O^{11}) on the hydroxyl group in the *R*-roscovitine complex. Therefore, very similar HB and, thus, more conservative binding patterns emerged in both the indirubin derivative and the *R*-roscovitine systems due to the bridge built by the water.

We also examined the conformational changes of Asp86 in all proteins and found that the oxygen atom (OD2), which was initially involved in the HB formation between Asp86 and the water, rotated by almost 90 ° in CDK5/indirubin-3′ oxime to an unfavorable HB formation direction.

To trace the motion of the water and to determine if any water-bridged HBs are formed or broken, ten crucial interatomic distances were monitored during the simulation. The initial interatomic distances and their average values after the simulations have stabilized are shown in Table 4. The first three distances of the table—the $O^{11'}$ of the inhibitor and the OD2 of the Asp86, the O^{w} of the water and the backbone O of the Gln130, and the $O^{11'}$ and the O^{w} of the water—show that the water molecule is almost at the center of the inhibitor, while the aspartic acid and the glutamine are at the beginning of the simulation. These three distances were monitored to track the motion of the water molecule. Figure 8a shows the changes in the three distances. It can be seen that the interatomic distances show significant changes until 350 ps, after which they oscillate about average values of 5.13, 2.94, and 2.79 Å. A comparison of these averaged values with the initial interatomic distances indicates that the water molecule remains relatively fixed between the inhibitor and the Gln, but moves away from the Asp. The other seven distances listed in Table 4 were monitored to study water-bridged HBs. Because of the movement of the water molecule, these distances change during the simulation. These seven distances also undergo changes in the first 350 ps. By taking 2.5 Å as the cutoff distance for HB to exist between oxygen and hydrogen [46], it is seen that HBs exist between the OD2 of the Asp and the H^2 of the water, and the O^{w} of the water and the H atom on the $O^{11'}H$ group at the start of the simulation. However, their average values after 350 ps show that HBs can only be established between the $O^{11'}$ of the inhibitor and the H^2 of the water and between the backbone O of the Gln130 and H^1 of the water. Only these two distances are shown in Fig. 8b for clarity. From this figure, it is seen that the HB between the inhibitor and the water molecule is quite stable after the initial 350 ps. However, the HB length between the water and the Gln130 keeps changing during the whole simulation process. Because the HB between the inhibitor and the water molecule is very stable and Fig. 8a already showed that the water molecule is located in the middle of the inhibitor and the Gln, continuous fluctuations in the HB length between the water and the Gln130 imply that the H^1 of the water keeps rotating around the O^{w}–H^2 axis. This is consistent with the reported descriptions on the characteristics of water molecules in proteins [47], which pointed out that water molecules keep translating and/or rotating during biological processes.

In many protein systems, water is an essential part of the 3-D structure, and its positions are similar for a family of proteins. [47–51] The conservation of internal water structure suggests that HB networks involved in binding are similar within protein families. Hence, detailed examinations of water locations were carried out on the results derived from both simulations and the observed crystal structures of CDK5 and CDK2-inhibitor complexes. However, the results show that such water molecules are located only in the crystal structures of CDK5/indirubin-3′-oxime and CDK2/indirubin-5-sulfonate (1E9H) reported by Davies et al. [38]. Our MM-PBSA results on the water-included and water-excluded CDK5/indirubin-3′-oxime complexes also helped to elucidate that the solvent molecule plays an important role in the binding. The relative free binding energies ($\Delta\Delta G^{calc}$) for the two CDK5 complexes were calculated and are listed in Table 5. The $\Delta\Delta G^{calc}$ values correctly mirror the rank scale of experimental values, $\Delta\Delta G^{exp}$ (IC_{50} 0.10, 0.16μM for indirubin-3′-oxime and *R*-roscovitine, respectively), only when the water molecule is considered. It is known that hydrogen bonding is dominated by electrostatic interactions, so forming one extra HB can definitely increase the electrostatic contribution to the binding between the donor and the acceptor. This is in agreement with the data in Table 5, which show that the E_{ele} of the water-excluded complexes are lower than those of water-included ones, indicating that electrostatic interactions are enhanced by about 10 kcal mol^{-1} when the water molecule binds with both the inhibitor and

Table 4 Interatomic distances of molecule pairs of the CDK5/indirubin-3′-oxime complex

Interatomic pair	Interatomic distance (Å)	
	Initial	Average after 350 ps
$O^{11'}$ … OD2	2.53	5.13
O … O^{W}	2.83	2.94
$O^{11'}$ … O	2.50	2.79
$O^{11'}$ … H^1	3.21	3.28
$O^{11'}$ … H^2	3.07	1.90
O … H	2.26	3.26
OD^2 … H^1	2.95	5.11
OD^2 … H^2	1.56	5.49
O … H^1	3.28	2.38
O … H^2	2.91	2.97

$O^{11'}$ is from the inhibitor as indicated in Fig. 1, OD2 is from Asp, O is from the backbone of Gln, H is the hydrogen of the hydroxyl group of the inhibitor, and O^{w}, H^1, and H^2 are from the water molecule

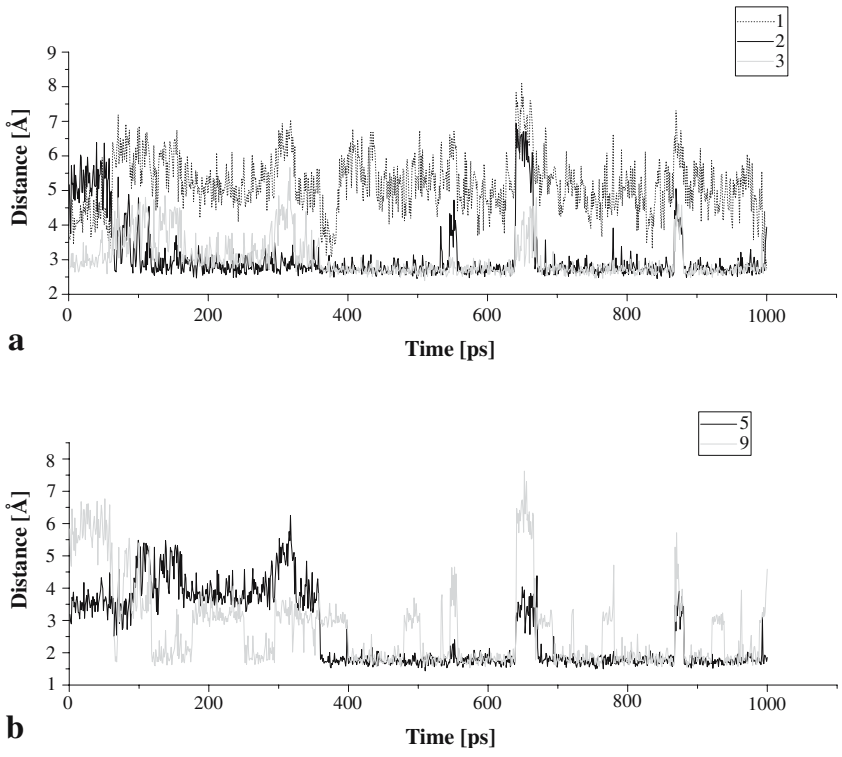

Fig. 8 **a** Distances between $O^{11'}$ of the inhibitor and the OD2 of the Asp86 (*1*), O of the water and backbone O of the Gln130 (*2*), $O^{11'}$ and O of the water (*3*). **b** Distances between $O^{11'}$ and the hydrogen atom H^2 of the bridging water (*5*) and O of the Gln130 and the H^1 of the water molecule (*9*)

the protein. We also note that the difference in E_{vdw} between the two complexes is not large, which implies that E_{vdw} is not influenced by the formation of the two HBs at the active site. Because of the increase in the E_{ele}, the ELE% of the water-included complex is improved to around 50%, suggesting that the electrostatic interactions contribute as much to the binding as the van der Waals interactions in the indirubin complex, unlike CDK5/*R*-roscovitine. Comparing the E_{ele} of both the roscovitine and indirubin complexes, it is seen that the difference between these two systems of about 3~4 kcal mol^{-1} is not as large as that between the water-included and water-excluded pairs (around 10 kcal mol^{-1}). This means that there is a weaker electrostatic interaction between the indirubin-3′-oxime and the CDK5 compared to that between the *R*-roscovitine and the kinase without the two water-connected HBs. This is consistent with the HB analysis of the CDK5/indirubin-3′-oxime complex, in which the third HB between the $N^{1'}$ of the inhibitor and the backbone oxygen of Leu83 does not contribute very favorably to the binding. Hence, the importance of this water molecule in the active site is clearly established.

We also investigated the van der Waals contributions in both CDK5/roscovitine and CDK5/indirubin systems and found that they are lower in the indirubin analogue complex. This can be explained from the difference in the chemical structures of these two inhibitors. As shown in Fig. 7, *R*-roscovitine and indirubin-3′-oxime approximately superimpose on the CDK5 active sites except that the indirubin derivative has an extra five-numbered ring and is more planar than the roscovitine structure. Although the extra ring generally implies more stacking interactions with the hydrophobic residues in the active site, roscovitine has more large, aliphatic substituents that stretch further and deeper out to the active site and can thus interact more effectively with the amino acids.

Finally, taking into account the conserved binding mode among these CDK systems, more data is needed to draw conclusions. We believe that water plays an important role in a CDK2/3′-substituted indirubin complex and should be included in the simulation. Because of the importance of the water molecule in the design of new indirubin-derived inhibitors, due consideration must be given to the interactions between ligand and the water. Therefore, the

Table 5 Results of MM-PBSA analyses of the CDK complexes with Indirubin-3′-oxime and *R*-roscovitine

Contribution	CDK5/indirubin-3′-oxime (with the water)	CDK5/indirubin-3′-oxime (without the water)	CDK5/*R*-roscovitine
E_{ele}	−32.19	−21.74	−28.01
E_{vdw}	−35.59	−38.56	−45.00
E_{np}	−3.39	−3.45	−4.46
E_{PB}	32.29	28.01	42.29
E_{sol}	28.90	24.56	37.82
E_{tot}	−38.89	−34.52	−35.27
$\Delta\Delta G^{exp}$ [a]		0.28	
$\Delta\Delta G^{calc}$		3.62	

E_{ele}, E_{vdw}, E_{np}, E_{PB}, E_{GB}, E_{sol}, and E_{tot} are electrostatic and van der Waals, nonpolar solvation, Poisson–Boltzmann, solvation and total energetic contributions (in kilocalories per mole), respectively for CDK5/Indirubin-3′-oxime with and without the HB network involving water and the CDK5/*R*-roscovitine complexes

[a] $\Delta\Delta G^{exp}$ is calculated from the IC_{50}: $\Delta\Delta G^{exp} = \Delta G^{CDK5}/\text{indirubin}-3-\text{oxine} - \Delta G^{CDK5}/\text{roscovitine} = RT \ln IC_{50 indirubin-3'-oxime} - RT \ln IC_{50 roscovitine}$

position of water molecules within the inhibitor, aspartic acid, glutamine, and the influence of the activating proteins on the CDKs are being investigated to obtain more detailed information. Currently, the location of water molecules in a protein structure can be determined routinely in single crystals by X-ray crystallography at a resolution of 2 Å or better [52]. Hence, more crystal structures of complexes with higher resolution can be expected, and these refined crystal structures will be able to verify positions of the water molecule in the CDK systems.

Conclusions

The different inhibitory levels in both CDK5 and CDK2 complexes with *R*-roscovitine cannot be explained by comparing the HB networks alone. Examinations on amino acid mutations revealed the reason for the higher inhibition efficiency of roscovitine on CDK5 than on CDK2. It is, thus, possible to obtain more efficient roscovitine-like inhibitors by modifying the structure of roscovitine to make the electrostatic field more complementary to the protein binding site. The electrostatic contribution to the binding energy was greatly improved because of the involvement of a water molecule in the CDK5/indirubin-3′-oxime complex, and the inclusion of a movable water molecule in the indirubin-3′-oxime system generated a similar binding mode to that in CDK5/*R*-roscovitine. Although such water molecules were not found in any other CDK5/inhibitor analogue complexes, water has the potential to enhance electrostatic interactions between the ligands and the protein. Therefore, more data is needed in the design of indirubin-like inhibitors.

Acknowledgement Prof. Laurent Meijer in France and Dr. Sung-Hou Kim in the USA are gratefully acknowledged for providing the crystal structures of the CDK2/*R*-roscovitine complex.

References

1. Norbury C, Nurse P (1992) Annu Rev Biochem 61:441–470
2. de Azevedo WF, Mueller-Dieckmann HJ, Schulze-Gahmen U, Worland PJ, Sausville E, Kim SH (1996) Proc Natl Acad Sci U S A 93:2735–2740
3. de Azevedo WF, Leclerc S, Meijer L, Havlicek L, Strnad M, Kim SH (1997) Eur J Biochem 243:518–526
4. Harper JW, Adams PD (2001) Chem Rev 101:2511–2526
5. Meyerson M, Enders GH, Wu CL, Su LK, Gorka C, Nelson C, Harlow E, Tsai LH (1992) EMBO J 11:2909–2917
6. Bu B, Li J, Davies P, Vincent I (2002) J Neurosci 22:6515–6525
7. Lau LF, Seymour PA, Sanner MA, Schachter JB (2002) J Mol Neurosci 19:267–273
8. Nguyen MD, Julien JP (2003) Neurosignals 12:215–220
9. Lau LF, Ahlijanian MK (2003) Neurosignals 12:209–214
10. Smith PD, Crocker SJ, Jackson-Lewis V, Jordan-Sciutto KL, Hayley S (2003) Proc Natl Acad Sci U S A 100:13650–13655
11. Sausville EA (2002) Trends Mol Med 8:S32–S37
12. Knockaert M, Greengard P, Meijer L (2002) Trends Pharmacol Sci 23:417
13. Crews CM, Mohan R (2000) Curr Opin Chem Biol 4:47–53
14. Sielecki TM, Boylan JF, Benfield PA, Trainor GL (2000) J Med Chem 43:1–18
15. Huew A, Mazitschek R, Giannis A (2003) Angew Chem Int Ed 42:2122–2138
16. Meijer L, Borgne A, Mulner O, Chong JP, Blow JJ, Inagaki N (1997) Eur J Biochem 243:527–536
17. Hoessel R, Leclerc S, Endicott JA, Nobel ME, Lawrie A, Tunnah P, Leost M, Damiens E, Marie D, Marko D, Niederberger E, Tang W, Eisenbrand G, Meijer L (1999) Nat Cell Biol 1:60–67
18. Mapelli M, Massimiliano L, Crovace C, Seeliger MA, Tsai LH, Meijer L, Musacchio A (2005) J Med Chem 48:671–679
19. Cavalli A, Dezi C, Folkers G, Scapozza L, Recanatini M (2001) Proteins 45:478–485
20. Otyepka M, Køí Z, Koèa J (2002) J Biomol Struct Dyn 20:141–154
21. de Azevedo WF Jr, Gaspar RT, Canduri F, Camera JC Jr, Silveira NJF (2002) Biochem Biophys Res Commun 297: 1154–1158
22. Cavalli A, Vivo MD, Recanatini M (2003) Chem Commun (Camb) 1308–1309
23. Sims PA, Wong CF, McCammon JA (2003) J Med Chem 46:3314–3325
24. Park H, Yeom MS, Lee S (2004) Chembiochem 5:1662–1672
25. Bártová I, Otyepka M, Køí Z, Koèa J (2004) Protein Sci 13:1449–1457
26. Bártová I, Otyepka M, Køí Z, Koèa J (2005) Protein Sci 14:445–451
27. Cornell WD, Cieplak P, Bayly CI, Gould IR, Merz KM, Ferguson DM Jr, Spellmeyer DC, Fox T, Caldwell JW, Kollman PA (1995) J Am Chem Soc 117:5179–5197
28. Besler BH, Merz KM, Kollman PA (1990) J Comput Chem 11:431–439
29. Fox T, Kollman PA (1998) J Phys Chem B 102:8070–8079
30. Case DA, Pearlman DA, Caldwell JW, Cheatham III TE, Wang J, Ross WS, Simmerling CL, Darden TA, Merz KM, Stanton RV, Cheng AL, Vincent JJ, Crowley M, Tsui V, Gohlke H, Radme RJ, Duan Y, Pitera J, Massova I, Seibel GL, Singh UC, Weiner PK, Kollman PA (2002) AMBER 7. University of California, San Francisco
31. Jorgensen WL, Chandrasekhar J, Madura JD, Impey RW, Klein ML (1983) J Chem Phys 79:926–935
32. Darden T, York D, Pedersen L (1993) J Chem Phys 98: 10089–10092
33. Ryckaert JP, Ciccotti G, Berendsen HJC (1977) J Comput Phys 23:327–341
34. Massova I, Kollman PA (2000) Perspect Drug Discov Des 18:113–135
35. Connolly ML (1983) J Appl Crystallogr 16:548–558
36. Sitkoff D, Sharp KA, Honig B (1994) J Phys Chem 98: 1978–1988
37. Stella L, Melchionna S (1998) J Chem Phys 109:10115–10123
38. Davies TG, Tunnah P, Meijer L, Marko D, Eisenbrand G, Endicott JA, Noble MEM (2001) Structure 9:389–397
39. Jautelat R, Brumby T, Schäfer M, Briem H, Eisenbrand G, Schwahn S, Krüger M, Lücking U, Prien O, Siemeister G (2005) Chembiochem 6:531–540
40. de Bondt HL, Rosenblatt J, Jancarik J, Jones HD, Morgan DO, Kim SH (1993) Nature 363:595–602
41. Schulze-Gahmen U, de Bondt HL, Kim SH (1996) J Med Chem 39:4540–4546
42. Lawrie AM, Noble MEM, Tunnah P, Brown NR, Johnson LN, Endicott JA (1997) Nat Struct Biol 4:796–801
43. Noble MEM, Endicott JA (1999) Pharmacol Ther 82:269–278
44. Brown NR, Noble MEM, Endicott JA, Johnson LN (1999) Nat Cell Biol 1:438–443
45. Arris CE, Boyle, FT, Calvert AH, Curtin NJ, Endicott JA, Garman EF, Gibson AE, Golding BT, Grant S, Griffin RJ, Jewsbury P, Johnson LN, Lawrie AM, Newell DR, Noble MEM, Sausville EA, Schultz R, Yu W (2000) J Med Chem 43:2797–2804
46. Lemaitre V, Ali R, Kim C, Watts A, Fischer WB (2004) FEBS Lett 563:75–81
47. Jeffrey GA, Saenger W (1991) Hydrogen bonding in biological structures. Springer, Berlin Heidelberg New York, pp 372–373

48. Baker EN, Hubbard RE (1984) Prog Biophys Mol Biol 44: 97–179
49. Bode W, Schwager P (1975) J Mol Biol 98:693–717
50. Sawyer L, Shotton DM, Campbell JW, Wendell PL, Muirhead H, Watson HC, Diamond R, Ladner RC (1978) J Mol Biol 118:137–208
51. Blake CCF, Pulford WCA, Artymiuk PJ (1983) J Mol Biol 167:693–723
52. Gottfried O, Edvards L (1995) Acc Chem Res 28:171–177